Journal Pre-proof

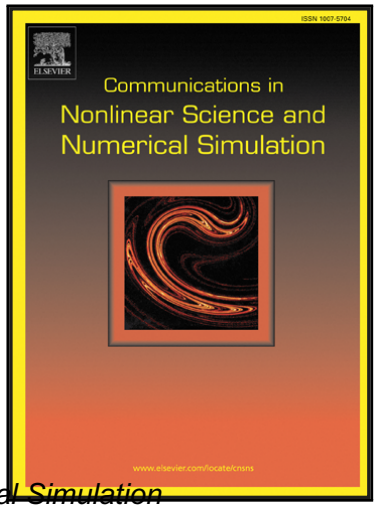

Hidden attractors and multistability in a modified Chua's circuit

Ning Wang, Guoshan Zhang, Kuznetsov N.V., Han Bao

PII: S1007-5704(20)30324-5
DOI: https://doi.org/10.1016/j.cnsns.2020.105494
Reference: CNSNS 105494

To appear in: *Communications in Nonlinear Science and Numerical Simulation*

Received date: 18 June 2020
Revised date: 7 August 2020
Accepted date: 12 August 2020

Please cite this article as: Ning Wang, Guoshan Zhang, Kuznetsov N.V., Han Bao, Hidden attractors and multistability in a modified Chua's circuit, *Communications in Nonlinear Science and Numerical Simulation* (2020), doi: https://doi.org/10.1016/j.cnsns.2020.105494

Highlights

- Presents a modified Chua's circuit with three stable node-foci and two unstable saddles.
- Hidden attractors have very small attraction basins not being connected with any fixed point.
- Hidden attractors coexist with point attractors in the entire period-doubling bifurcation route.
- Circuit simulations and DSP-assisted experiments validate the hidden attractors and multistability.

Hidden attractors and multistability in a modified Chua's circuit

Ning Wang[a], Guoshan Zhang[a,*], Kuznetsov N. V.[b,c,d], Han Bao[e]

[a] *School of Electrical and Information Engineering, Tianjin University, Tianjin 300072, China*
[b] *Faculty of Mathematics and Mechanics, St. Petersburg State University, Peterhof, St. Petersburg 198504, Russia*
[c] *Department of Mathematical Information Technology, University of Jyväskylä, Jyväskylä 40014, Finland*
[d] *Institute for problems in Mechanical Engineering of the Russian Academy of Sciences, St. Petersburg 199178, Russia*
[e] *College of Automation Engineering, Nanjing University of Aeronautics and Astronautics, Nanjing 210016, China*

Abstract

The first hidden chaotic attractor was discovered in a dimensionless piecewise-linear Chua's system with a special Chua's diode. But designing such physical Chua's circuit is a challenging task due to the distinct slopes of Chua's diode. In this paper, a modified Chua's circuit is implemented using a 5-segment piecewise-linear Chua's diode. In particular, the coexisting phenomena of hidden attractors and three point attractors are noticed in the entire period-doubling bifurcation route. Attraction basins of different coexisting attractors are explored. It is demonstrated that the hidden attractors have very small basins of attraction not being connected with any fixed point. The PSIM circuit simulations and DSP-assisted experiments are presented to illustrate the existence of hidden attractors and coexisting attractors.

Keywords: Chua's diode; Chua's circuit; Chaos; Hidden attractor; Initial condition; Multistability; Attraction basin

1. Introduction

For many years, it has been generally accepted that the attraction basin of an attractor is connected with system's unstable equilibrium, and thus initial orbits starting from the unstable manifold of a neighborhood of equilibrium can easily reach the oscillation. However, some counterexamples were found in dynamical systems, in which the attraction basins of the attractors do not intersect with neighborhoods of unstable equilibria (if exists) and are located far away from such points [1]. This category of attractors are difficult to be located via standard procedure of compute simulation and are defined as hidden attractors. Recently, it has been shown that hidden attractors are connected with the multistability phenomenon [2, 3]. A variety of dynamical systems with multistability and hidden attractors have been discovered [4–10]. Some dynamical systems with only stable equilibrium, stable line equilibrium, or with no equilibrium are intentionally and easily constructed for generating hidden attractors [11]. By contrast, finding hidden attractors in physical systems is difficult as system itself has specific physical properties cannot be changed arbitrarily [12]. Thus, finding hidden attractors and identifying the dynamics of such systems is a challenging work.

Chua's circuit is the first electronic circuit exhibiting chaos and provided the evidence of the existence of chaos in the physical world [13]. In 2010, Leonov and Kuznetsov discovered the first hidden chaotic attractor in Chua's system with piecewise-linear Chua's diode [14–16]. Afterwards, hidden chaotic attractor was also demonstrated in a modified Chua's system with a smooth nonlinearity [17]. In 2014, Li et al. restudied the Chua's system proposed in [16] and shown that twin hidden attractors can coexist in this system for some parameters [18]. In 2017, Zhao et al. reported the coexistence of stable equilibria and hidden periodic limit cycle in a modified smooth Chua's system [19]. All these results, without exception,

*Corresponding author
Email addresses: cczuwangning@163.com (Ning Wang), zhanggs@tju.edu.cn (Guoshan Zhang), nkuznetsov239@gmail.com (Kuznetsov N. V.), charlesbao0319@gmail.com (Han Bao)

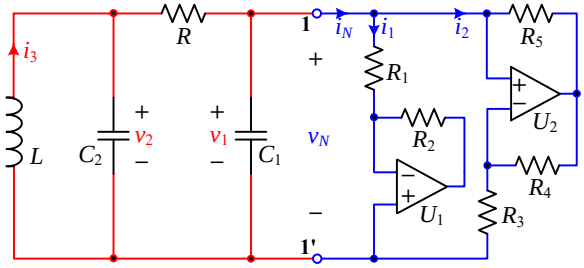

Figure 1: Chua's circuit with modified Chua's diode.

Table 1: Parameters of the modified Chua's circuit

Parameters	Significations	Values
C_1	Capacitance	12 nF
C_2	Capacitance	96 nF
L	Inductance	18.5 mH
R	Resistance	1.7 kΩ
R_1	Resistance	1 kΩ
R_2	Resistance	7.5 kΩ
R_3	Resistance	880 Ω
R_4 R_5	Resistance	200 Ω
E_{sat}	Saturation output voltage of U_1 and U_2	13 V

were found based on dimensionless Chua's systems of coupled ODEs, rather than practical electronic circuits. It was expected to expand this research in practical circuits.

Further observations of hidden Chua's attractors in physical circuits were presented sequentially [20–24]. A comprehensive review and study of scenario of the hidden Chua's attractors were collated by Stankevich et al. [25]. The above mentioned Chua's circuit variants vary in a large range. In [20], the use of a first-order hybrid Chua's diode made the whole system to be fourth-order. In [21], the authors only taken the inner three segments of 3-NIC-based Chua's diode into consideration and omitted the dynamics caused by other potential segments [21]. The system proposed in [23] employed two nonlinearities implemented by one-stage op-amp-based NIC and two anti-parallel diodes, respectively. In [24], the Chua's nonlinearity was implemented by using the 'Arbitrary Source' (voltage-controlled current source) instead of a practical implementation. To better identify the hidden dynamics of the Chua's circuit, it is meaningful to design a piecewise-linear Chua's diode with desired segments. For this purpose, a modified Chua's circuit with a 5-segment piecewise-linear Chua's diode is presented, in which hidden attractors and coexisting attractors are identified.

The remainder of the paper is organized as follows. In Section 2, the circuit description and basic properties analyses are performed. Dynamics analyses and simulations are presented in Section 3. The PSIM circuit simulations and DSP-assisted verifications are provided in Section 4. The last section concludes the paper.

2. Modified Chua's circuit

In this section, we first propose a modified Chua's diode with 5-segment piecewise-linearity. Using the Chua's diode, a Chua's circuit with three stable node-foci and two unstable saddles is further implemented, as shown in Fig. 1.

2.1. Design of Chua's doide

As Chua's diode is the part of Chua's circuit forming activity and nonlinearity of the whole system, changing its characteristics is an effective way to generate different types of attractors, e.g. hidden at-

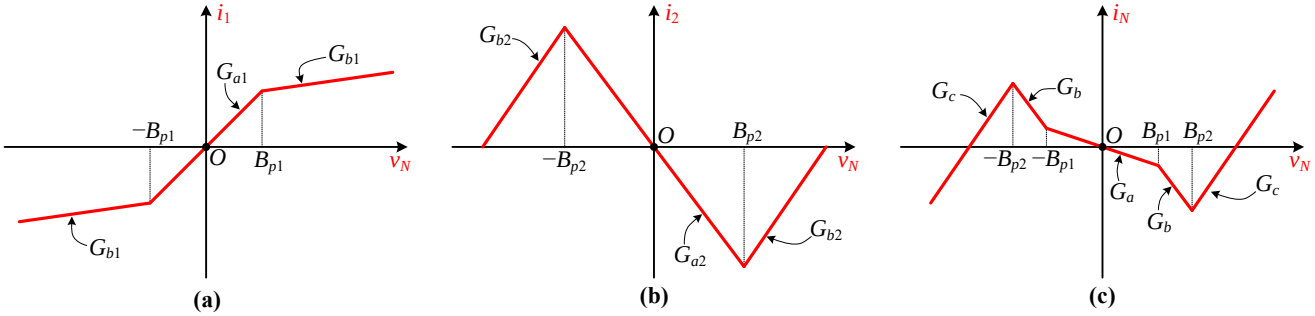

Figure 2: The $v-i$ characteristic curves of three nonlinear resistors with different nonlinearities **(a)** nonlinear resistor with positive inner segment slope and outer segment slope **(b)** nonlinear resistor with negative inner segment slope and positive outer segment slope **(c)** modified 5-segment piecewise-linear Chua's diode via parallel connection of the first two nonlinear resistors.

tractors [16, 25] or multi-scroll attractors [26]. For piecewise-linear Chua's diode, the breakpoints and slopes are important parameters determining their characteristics. The most classical implementation of piecewise-linear Chua's diode is the parallel connection of two op-amp-based negative impedance converters (NIC) [13].

In dimensionless Chua's equations, the segment slopes and breakpoints of Chua's nonlinearity can be arbitrarily set. But the parameters of Chua's diode in practical Chua's circuit are interrelated. The saturation output voltages of the op-amps are constant when fixing power supplies, which means that the breakpoints can only be adjusted by resistors. Meanwhile, the variation of resistance will result in a change of segment slopes. In order to achieve the desired segment slopes and breakpoints, the Chua's diode should be implemented in subtle ways. Thus, we consider the following two existing nonlinear resistors to design a new Chua's diode.

Comprehensive review of two nonlinear resistors. In [26], a passive nonlinear resistor with positive inner segment slope and outer segment slope is designed. The implemented circuit of such nonlinear resistor only contains two linear resistors R_1, R_2, and one op-amp U_1, as shown in the right part of the port '$1-1'$' of Fig. 1. The $v-i$ characteristic of the nonlinear resistor is featured by three parameters and represented as

$$i_1 = h_1(v_N) = G_{b1}v_N + 0.5(G_{a1} - G_{b1})(|v_N + B_{p1}| - |v_N - B_{p1}|), \tag{1}$$

where

$$G_{a1} = \frac{1}{R_1}, G_{b1} = \frac{1}{R_1 + R_2}, B_{p1} = \frac{R_1}{R_2}E_{\text{sat}}$$

denote the inner slope, outer slope, and breakpoint, respectively. Fig. 2(a) plots the $v-i$ characteristic curve, in which two slopes satisfy $G_{a1} > G_{b1} > 0$.

Another nonlinear resistor with negative inner segment slope and positive outer segment slope is proposed in [22]. The implemented circuit is a saturated NIC containing three linear resistors R_3, R_4, R_5, and one op-amp U_2, as shown in the most right part of Fig. 1. As the use of saturation output property of the op-amp, the nonlinear resistor shows piecewise-linearity. The $v-i$ characteristic of the nonlinear resistor is represented as

$$i_2 = h_2(v_N) = G_{b2}v_N + 0.5(G_{a2} - G_{b2})(|v_N + B_{p2}| - |v_N - B_{p2}|), \tag{2}$$

where G_{a2}, G_{b2}, and B_{p2} are the inner slope, outer slope, and breakpoint, respectively. When $R_4 = R_5$, one has

$$G_{a2} = -\frac{1}{R_3}, G_{b2} = \frac{1}{R_4}, B_{p2} = \frac{R_3}{R_3 + R_4}E_{\text{sat}}.$$

Fig. 2(b) plots the $v-i$ curve of the nonlinear resistor, in which the slopes satisfy $G_{a2} < 0$ and $G_{b2} > 0$.

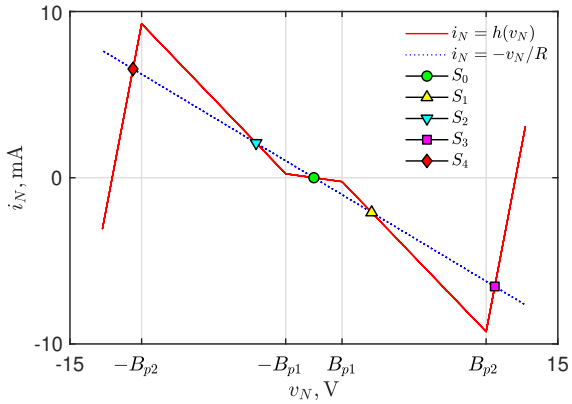

Figure 3: The $v-i$ characteristic of the proposed Chua's diode expressed by (3), where the 5 intersection points of the piecewise-linear curve and the straight load line indicate 5 equilibira of system (6).

New 5-segment piecewise-linear Chua's diode. By parallel connecting the above two nonlinear resistors, a new piecewise-linear Chua's diode can be designed. When $B_{p2} \neq B_{p1}$, the $v-i$ curve of the new Chua's diode is 5-segment piecewise-linear, expressed as

$$\begin{aligned} i_N = h(v_N) = G_c v_N &+ 0.5(G_a - G_b)(|v_N + B_{p1}| - |v_N - B_{p1}|) \\ &+ 0.5(G_b - G_c)(|v_N + B_{p2}| - |v_N - B_{p2}|), \end{aligned} \tag{3}$$

where G_a, G_b, G_c, B_{p1}, and B_{p2} are the inner slope, middle slope, outer slope, inner breakpoint, and outer breakpoint, respectively. Specifically, the five parameters are

$$\begin{aligned} G_a &= G_{a1} + G_{a2} = \frac{1}{R_1} - \frac{1}{R_3}, \\ G_b &= G_{b1} + G_{a2} = \frac{1}{R_1 + R_2} - \frac{1}{R_3}, \\ G_c &= G_{b1} + G_{b2} = \frac{1}{R_1 + R_2} + \frac{1}{R_4}, \\ B_{p1} &= \frac{R_1}{R_2} E_{\text{sat}}, \\ B_{p2} &= \frac{R_3}{R_3 + R_4} E_{\text{sat}}. \end{aligned} \tag{4}$$

When $B_{p2} > B_{p1}$ and $-G_{a2} > G_{a1}$, the $v-i$ curve is shown in Fig. 2(c). It is found from Fig. 2(c) that the slopes G_a and G_b of the inner three segments are negative and satisfy $G_a > G_b$, which has the similar characteristic with the Chua's diode in [16]. We here choose the circuit parameters of Fig. 1 as listed in Table 1. The specific parameters of (4) are

$$\begin{aligned} &G_a = -0.1364\,\text{mS}, G_b = -1.0187\,\text{mS}, G_c = 5.1176\,\text{mS}, \\ &B_{p1} = 1.7333\,\text{V}, B_{p2} = 10.5926\,\text{V}. \end{aligned} \tag{5}$$

The $v-i$ characteristic of the proposed Chua's diode. To simulate the $v-i$ curve of the modified Chua's diode, the sinusoidal function $v_N = V_{\text{m}}\sin(2\pi ft)$ with $V_{\text{m}} = 13\,\text{V}$ and $f = 100\,\text{Hz}$ is used as the driven signal. When the parameters in Table 1 are used, the simulated loci in the $v_N - i_N$ plane is shown in Fig. 3. The negative inner segment slopes satisfy $|G_a| < |G_b|$, which is completely different from that of the classical Chua's diode satisfying $|G_a| > |G_b|$ [13]. Besides, the modified Chua's diode has simpler implementation than that reported in [21].

2.2. Circuit state equation

The state equations of Fig. 1 are written as

$$\begin{cases} \dfrac{\mathrm{d}v_1}{\mathrm{d}t} = -\dfrac{v_1}{RC_1} + \dfrac{v_2}{RC_1} - \dfrac{h(v_1)}{C_1}, \\ \dfrac{\mathrm{d}v_2}{\mathrm{d}t} = \dfrac{v_1}{RC_2} - \dfrac{v_2}{RC_2} + \dfrac{i_3}{C_2}, \\ \dfrac{\mathrm{d}i_3}{\mathrm{d}t} = -\dfrac{v_2}{L}, \end{cases} \tag{6}$$

where $h(v_1)$ is the Chua's nonlinearity expressed by (3). The system is invariant under the transformation $(v_1, v_2, i_3) \leftrightarrow (-v_1, -v_2, -i_3)$, i.e., it is symmetric about origin.

2.3. Equilibrium point and stability

To calculate the DC equilibria of the modified Chua's circuit, let three equations of (6) be zero. It is easy to obtain

$$-\frac{v_1}{R} = h(v_1) = i_3, \text{and } v_2 = 0. \tag{7}$$

The first equation of (7) means that the solutions of $-v_1/R = h(v_1)$ can be calculated by the intersections between the Chua's nonlinearity $h(v_1)$ and the load line $-v_1/R$. When $G_b + (G_a - G_b)B_{p1}/B_{p2} < -1/R < G_a$ (i.e., $1.1437\,\mathrm{k\Omega} < R < 7.3333\,\mathrm{k\Omega}$), the circuit has five equilibria.

As the Chua's diode is piecewise-linear, system (6) has nonsmooth points (i.e., the breakpoints), where the Jacobian matrix is not defined. The circuit equation can be separated into five sub-equations for each segment by planes $v_1 = B_{p1}$, $v_1 = -B_{p1}$, $v_1 = B_{p2}$, and $v_1 = -B_{p2}$. The corresponding five distinct affine regions are

$$\begin{cases} D_0 = \{(v_1, v_2, i_3) \mid -B_{p1} \le v_1 \le B_{p1}\}, \\ D_1 = \{(v_1, v_2, i_3) \mid B_{p1} < v_1 \le B_{p2}\}, \\ D_2 = \{(v_1, v_2, i_3) \mid -B_{p2} \le v_1 < -B_{p1}\}, \\ D_3 = \{(v_1, v_2, i_3) \mid v_1 > B_{p2}\}, \\ D_4 = \{(v_1, v_2, i_3) \mid v_1 < -B_{p2}\}. \end{cases} \tag{8}$$

Then the equilibria in each of the above subsets are calculated as

$$\begin{cases} S_0 = (0, 0, 0), \\ S_{1,2} = (\pm RI_1, 0, \mp I_1), \\ S_{3,4} = (\pm RI_2, 0, \mp I_2), \end{cases} \tag{9}$$

where

$$I_1 = \frac{(G_b - G_a)B_{p1}}{1 + RG_b},$$
$$I_2 = \frac{(G_b - G_a)B_{p1} + (G_c - G_b)B_{p2}}{1 + RG_c}.$$

The stability condition here is investigated for each linear parts of D_0, $D_{1,2}$, and $D_{3,4}$. The matrices of linearizations at the corresponding equilibria have the form

$$\mathbf{J} = \begin{bmatrix} -\frac{1}{RC_1} - \frac{H}{C_1} & \frac{1}{RC_1} & 0 \\ \frac{1}{RC_2} & -\frac{1}{RC_2} & \frac{1}{C_2} \\ 0 & -\frac{1}{L} & 0 \end{bmatrix}, \tag{10}$$

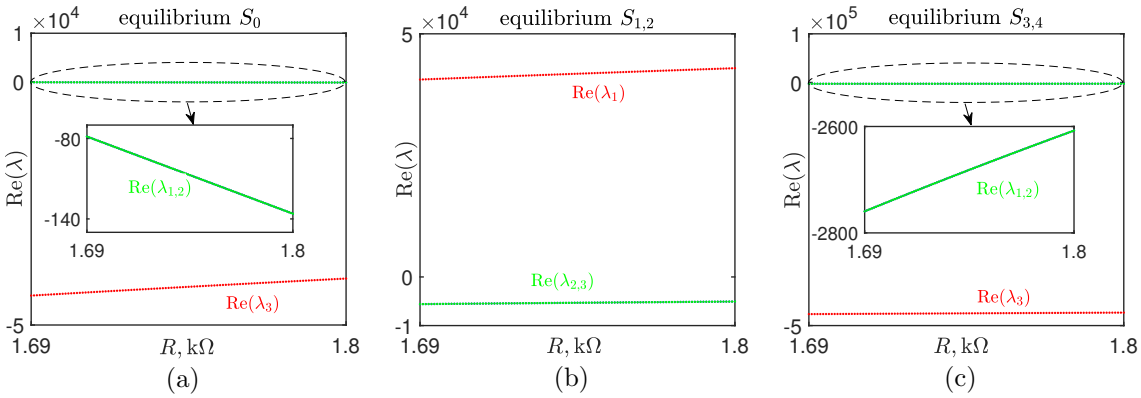

Figure 4: The real parts loci of the eigenvalues of (11) for $R \in [1.69\,\mathrm{k\Omega}, 1.8\,\mathrm{k\Omega}]$, and other parameters fixed in Table 1 **(a)** for the equilibrium S_0 **(b)** for the equilibria $S_{1,2}$ **(c)** for the equilibria $S_{3,4}$.

where $H = G_a$ for S_0 in the D_0 region, $H = G_b$ for $S_{1,2}$ in the $D_{1,2}$ regions, and $H = G_c$ for $S_{3,4}$ in the $D_{3,4}$ regions, respectively.

The characteristic equation at the equilibrium is

$$P(\lambda) = \det(\mathbf{1}\lambda - \mathbf{J}) = \lambda^3 + a_1\lambda^2 + a_2\lambda + a_3 = 0, \tag{11}$$

where

$$\begin{aligned} a_1 &= \frac{1+RH}{RC_1} + \frac{1}{RC_2}, \\ a_2 &= \frac{1}{LC_2} + \frac{H}{RC_1C_2}, \\ a_3 &= \frac{1+RH}{RLC_1C_2}. \end{aligned}$$

The Routh-Hurwitz conditions for the cubic polynomial are given by

$$\begin{cases} a_1 = \dfrac{1+RH}{RC_1} + \dfrac{1}{RC_2} > 0, \\ a_3 = \dfrac{1+RH}{RLC_1C_2} > 0, \\ a_1a_2 - a_3 = \dfrac{LH(C_1+C_2) + RLC_2H^2 + RC_1^2}{R^2LC_1^2C_2^2} > 0. \end{cases} \tag{12}$$

Here, stability condition will be discussed in the parameter interval $R \in [1.69\,\mathrm{k\Omega}, 1.8\,\mathrm{k\Omega}]$, which are related with the hidden dynamics to be considered in the following sections. With the parameters in Table 1 and $R \in [1.69\,\mathrm{k\Omega}, 1.8\,\mathrm{k\Omega}]$, one has:

- For the equilibrium S_0, $H = G_a$. Because $1 + RG_a > 0$, the first two conditions of (12) are obviously satisfied. Besides, due to $LG_a(C_1 + C_2) + RLC_2G_a^2 + RC_1^2 > 0$, the third condition of (12) is satisfied as well. Thus, S_0 is stable.
- For the equilibria $S_{1,2}$, $H = G_b$. In view of $1 + RG_b < 0$, the second condition of (12) is not satisfied. Thus, $S_{1,2}$ are two unstable equilibria.
- For the equilibria $S_{3,4}$, $H = G_c$. Due to $G_c > 0$, the three conditions of (12) are all satisfied for any positive parameters of Table 1, implying that $S_{3,4}$ are always stable.

With the parameters in Table 1, the eigenvalues associated with five equilibria are calculated as

$$\begin{cases} S_0 : \lambda_{1,2} = -84 \pm \mathrm{j}22048, \lambda_3 = -43616, \\ S_{1,2} : \lambda_1 = 40819, \lambda_{2,3} = -5536 \pm \mathrm{j}21545, \\ S_{3,4} : \lambda_{1,2} = -2745 \pm \mathrm{j}23554, \lambda_3 = -476128. \end{cases} \tag{13}$$

Hence S_0 and $S_{3,4}$ are three stable node-foci, whereas $S_{1,2}$ are two symmetric unstable saddles.

When the resistance R is chosen as an adjustable parameter, it has a wide parameter interval in which the equilibria S_0 and $S_{3,4}$ are always three stable node-foci, and another two equilibria $S_{1,2}$ are always unstable saddles. Using the parameters that listed in Table 1, the numerical solutions of the eigenvalues of (11) for $R \in [1.69\,\mathrm{k\Omega}, 1.8\,\mathrm{k\Omega}]$ are shown in Fig. 4. It is found from Fig. 4(a) and (c) that the real parts of the eigenvalues of (11) for the equilibria S_0 and $S_{3,4}$ are always negative, thus these three equilibria are stable for $R \in [1.69\,\mathrm{k\Omega}, 1.8\,\mathrm{k\Omega}]$. However, Fig. 4(b) shows that there always exists one eigenvalue with positive real part for the equilibria $S_{1,2}$, implying unstable state.

3. Numerical simulations of dynamical behaviors

In this section, we investigate the phase portraits, bifurcation diagrams, and attraction basins using numerical simulations. Fourth-order Runge-Kutta algorithm with time step of $2\,\mu\mathrm{s}$ is used.

3.1. Hidden chaotic attractor

The modified Chua's circuit has multiple stable and unstable equilibria. It is different from the multi-scroll Chua's circuit with only unstable equilibria [26] and the Chua's circuit with two stable node-foci and one saddle [22]. Referring to the Chua's nonlinearity reported in [16], it is possible to generate hidden attractor from the modified Chua's circuit via configuring appropriate parameters and special initial states.

Using the parameters in Table 1 and different initial conditions (ICs), four different attractors are simulated in Fig. 5(a). It is found that the orbits starting from ICs $(4, -2, 0)$, $(6, 3, 0)$, $(-6, -3, 0)$ are asymptotically stable to equilibria S_0, S_3 and S_4, finally form three point attractors $\mathcal{A}_1$, $\mathcal{A}_2$ and $\mathcal{A}_3$. The orbit starting from IC $(0, -1.9, 0)$ demonstrate a chaotic attractor $\mathcal{A}_4$. Attraction basin is an effective tool to search and visualize hidden attractors in the phase space [27]. The corresponding attraction basins in different sections are plotted in Fig. 5(b), (c), and (d), respectively. The cyan, yellow, and blue basins correspond to the point attractors that located in the equilibria S_4, S_3, and S_0, respectively. The orange basin does not intersect with small neighborhoods of all equilibria and corresponds to a hidden attractor, in which the black orbits are the cross section of the hidden attractor.

3.2. Bifurcation diagrams

Two-parameter bifurcation. We first compute two-parameter bifurcation diagrams to show parameter-related dynamical behaviors of the Chua's circuit. Due to the existence of stable equilibria, it is believed that the orbits excited from the small neighborhoods of these stable equilibria will asymptotically converge to the equilibria. In order to compute the potential bifurcation diagram with complex dynamics, some special initial values being located far away from the small neighborhoods of stable equilibria are configured.

The initial conditions we used here are $v_1(0) = 0\,\mathrm{V}$, $v_2(0) = 1.9\,\mathrm{V}$, and $i_3(0) = 0\,\mathrm{A}$. Besides, the nonlinearity of the Chua's diode is expected to be unchanged, thus the parameters of Chua's diode are fixed. The two-dimensional bifurcation diagrams of Fig. 6 show rich dynamical behaviors in different two-parameter spaces. The numbers in colorbar indicate the periodicity, dynamical areas marked by P_0 and CH indicate point attractor and chaos, respectively. From Fig. 6, different periodic and chaotic areas, routes to chaos via period-doubling bifurcation, and complex bifurcation boundaries are easily identified.

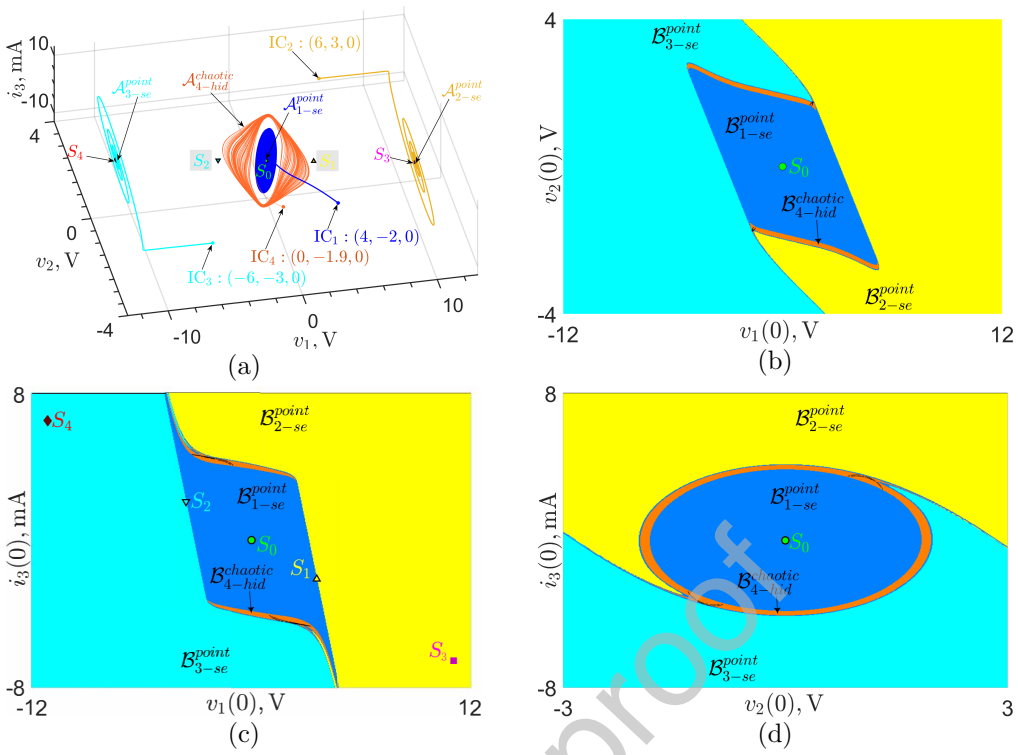

Figure 5: Coexistence of points and hidden chaotic attractor and their attraction basins, where the attractors are excited from different initial conditions (IC) with fixed parameters in Table 1. The cyan, yellow, and blue basins correspond to the point attractors located in the equilibria S_4, S_3, and S_0, respectively. The orange basin does not intersect with a neighborhood of all equilibria and corresponds to a hidden chaotic attractor, in which the black orbits are the cross section of the hidden attractor **(a)** phase portraits of different coexisting attractors **(b)** attraction basin for the section $i_3(0) = 0$ **(c)** attraction basin for the section $v_2(0) = 0$ **(d)** attraction basin for the section $v_1(0) = 0$.

Coexisting bifurcations. To compute a single-parameter bifurcation diagram, we trace the dynamics for the interval marked by the white dotted line in Fig. 6, i.e., $C_1 = 12\,\mathrm{nF}$, $C_2 = 96\,\mathrm{nF}$, $L = 18.5\,\mathrm{mH}$, and $R \in [1.69\,\mathrm{k\Omega}, 1.8\,\mathrm{k\Omega}]$. Taking the coexisting attractors and basin attractions in Section 3.1 into consideration, different initial conditions are set to show the coexisting bifurcations. Here, we choose five sets of ICs $(0, \pm 1.9, 0)$, $(\pm 6, \pm 3, 0)$, and $(4, -2, 0)$ to plot the local maxima of v_1 versus parameter R. The corresponding bifurcation diagrams are shown in Fig. 7.

It is found from Fig. 7(a) that with the decrease of parameter R, system (6) shows the period-doubling bifurcation route to chaos. Especially, for $R \in [1.7103\,\mathrm{k\Omega}, 1.7594\,\mathrm{k\Omega}]$, system (6) undergoes coexisting chaos, coexisting period-16, -8, -4, -2 and -1 states, respectively. When R decrease to $1.7103\,\mathrm{k\Omega}$, the coexisting chaotic orbits disappear and manifest robust chaos. When R increase to $1.7594\,\mathrm{k\Omega}$, two symmetric period-1 limit cycles merge into a single limit cycle. For $R \in [1.69\,\mathrm{k\Omega}, 1.695\,\mathrm{k\Omega}] \cup [1.7913\,\mathrm{k\Omega}, 1.8\,\mathrm{k\Omega}]$, the oscillations disappear and form point attractor located in the origin. The corresponding largest finite-time Lyapunov exponents with IC $(0, 1.9, 0)$ are calculated on time interval $[0, 0.2\,\mathrm{s}]$ and shown in Fig. 7(a) (see the green orbits). The consistence between the Lyapunov exponents and the bifurcation diagrams just emulate the rich dynamics of period-doubling bifurcation route and chaos in system (6).

In Fig. 7(b), the bifurcation orbits v_{1max} excited by ICs $(\pm 6, \pm 3, 0)$ and $(4, -2, 0)$ asymptotically converge to the equilibria S_3, S_4, and S_0, respectively, and finally form three point attractors. With R increasing, the point attractors located in S_3 and S_4 are keeping away from the origin, the specific locations can be calculated by (9). For these three sets of ICs, the largest Lyapunov exponents are all negative, indicating asymptotically converge motions.

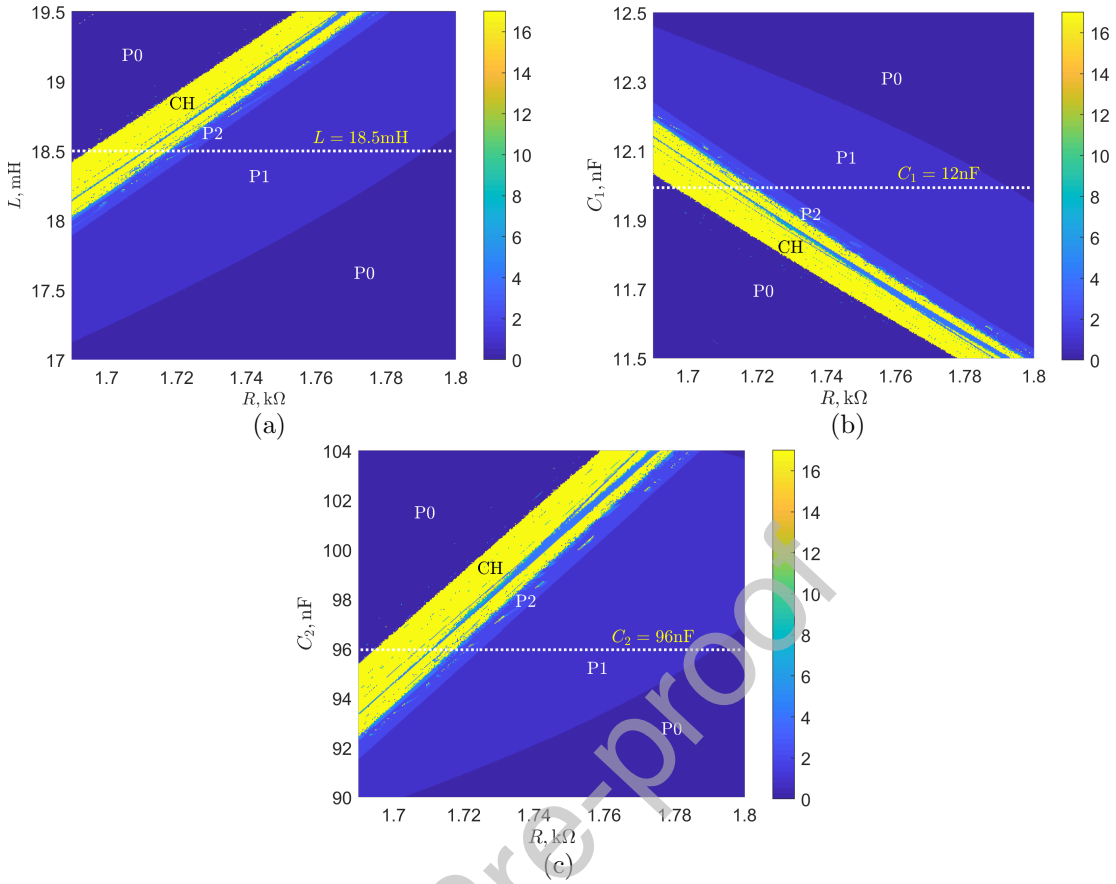

Figure 6: Two-parameter bifurcation diagrams **(a)** in the $R-L$ plane for $C_1 = 12\,\text{nF}$ and $C_2 = 96\,\text{nF}$ **(b)** in the $R-C_1$ plane for $C_2 = 96\,\text{nF}$ and $L = 18.5\,\text{mH}$ (c) in the $R-C_2$ plane for $C_1 = 12\,\text{nF}$ and $L = 18.5\,\text{mH}$, where the periodicity corresponds to the number in colourbar, P_0 and CH indicates point attractor and chaos, respectively.

3.3. Coexisting attractors and attraction basins

As the definition of hidden attractor makes clear, numerical check of the attraction basins and equilibria (if exists) is the most direct way for attractor identification. Especially, for dynamical system owing multiple stable and unstable equilibria (e.g., in the Rabinovich-Fabrikant system [27], two equilibria are stable but another three ones are unstable for the parameters $a = 0.1$ and $b = 0.2876$), visualization of the attraction basins of all attractors is particularly important.

System (6) has five equilibria including three stable node-foci and two unstable saddles. All five equilibria are located in the plane $v_2 = 0$, which is identified by (9). In order to explore the high quality graphics of attraction basins, the section $v_2(0) = 0$ with 360000 pixel points are used. Besides, the IC space $v_1(0) \times i_3(0) = (-5\,\text{V}, 5\,\text{V}) \times (-8\,\text{mA}, 8\,\text{mA})$ are considered to plot attraction basins in the neighborhoods of unstable equilibria. When choosing R as $1.78\,\text{k}\Omega$, $1.74\,\text{k}\Omega$, $1.72\,\text{k}\Omega$, $1.7185\,\text{k}\Omega$, $1.716\,\text{k}\Omega$ and $1.7\,\text{k}\Omega$, attraction basins of different coexisting attractors are presented in Fig. 8. As shown in Fig. 8, attraction basins of point attractors that being located in the equilibria S_4, S_3, and S_0 are marked by cyan, green, and blue, respectively. These three attraction basins are relatively big and almost occupy the whole section space. In contrast, the hidden attractors have very small attraction basins marked by orange/yellow. According to (9), it is calculated and shown that the locations of all five equilibria are far away from the orange/yellow attraction basins. Consequently, it will be very difficult to reach the oscillations when choosing initial values near any equilibrium point.

The local detail views of the hidden attractors overplotted on corresponding attraction basins are presented in Fig. 9. It is seen from Fig. 9(a) that there emerges oscillation of a single period-1 limit

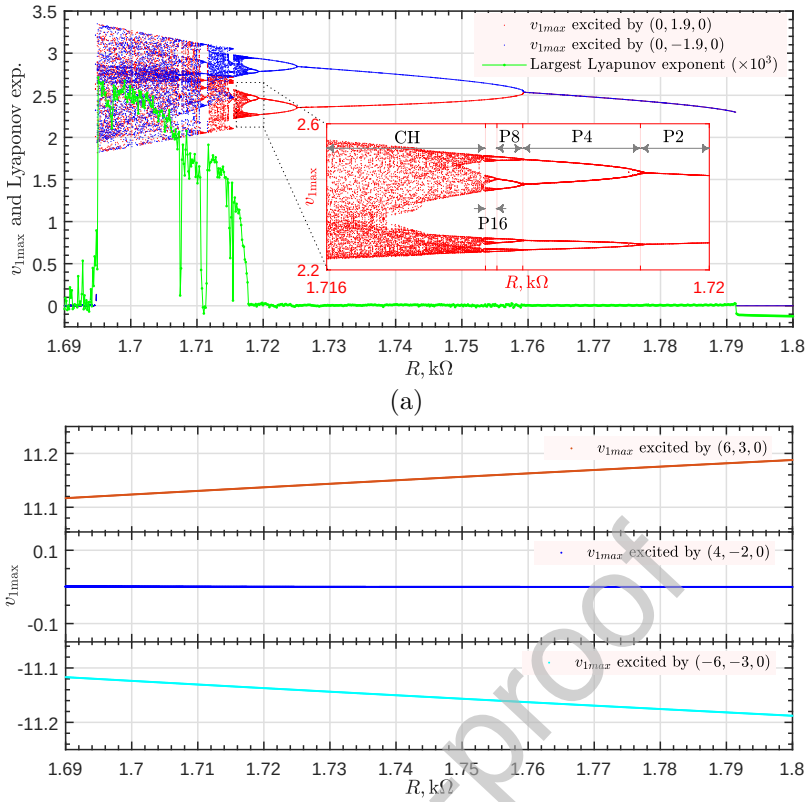

Figure 7: Bifurcation diagrams with respect to R, where the typical parameters in Table 1 are used. **(a)** v_{1max} excited by two sets of initial conditions $(0, \pm 1.9, 0)$ and the largest finite-time Lyapunov exponent spectra excited by IC $(0, 1.9, 0)$ **(b)** v_{1max} excited by three sets of initial conditions $(\pm 6, \pm 3, 0)$ and $(4, -2, 0)$.

cycle for $R = 1.78\,\mathrm{k}\Omega$. Afterwards, coexisting oscillations occur and arise twin period-1 limit cycles for $R = 1.74\,\mathrm{k}\Omega$. Correspondingly, the attraction basin of the original single limit cycle is split into two complex basins, as shown in Fig. 9(b). Fig. 9(c), (d), and (e) show the similar attraction basins, for which system undergoes the coexisting period-doubling bifurcation routes and generates twin period-2 limit cycles (for $R = 1.72\,\mathrm{k}\Omega$), twin period-4 limit cycles (for $R = 1.7185\,\mathrm{k}\Omega$), and twin chaotic attractor (for $R = 1.716\,\mathrm{k}\Omega$), respectively. With R decreasing, the twin chaotic attractors merge into a single hidden chaotic attractor. Local view of the hidden attractor overplotted on corresponding attraction basin is shown in Fig. 9(f).

Summarizing, all equilibria of the modified Chua's circuit are not intersect with the attraction basins of hidden attractors. Moreover, the coexisting phenomena of hidden attractors and three point attractors are noticed in the entire period-doubling bifurcation route. Up to five coexisting attractors exist in this Chua's circuit. Review the existing studies on multistability of Chua's system, this is the maximum number of coexisting attractors (including the self-excited and hidden attractors) that can be generated in the Chua's system [22, 25].

4. Circuit simulations and DSP-assisted validations

Some circuit simulation platforms, for examples, NI Multisim [26, 28], Pspice [29–31], and PSIM [21, 32] et al. are widely used to validate the dynamics of nonlinear circuits. Especially, PSIM can provide effective operation environments for verifications of initial condition-induced coexisting behaviors. When analog circuit experiment is carried, it is easy to obtain the three point attractors as they have big attraction basins being connected with corresponding equilibria. However, the hidden attractors have very small attraction

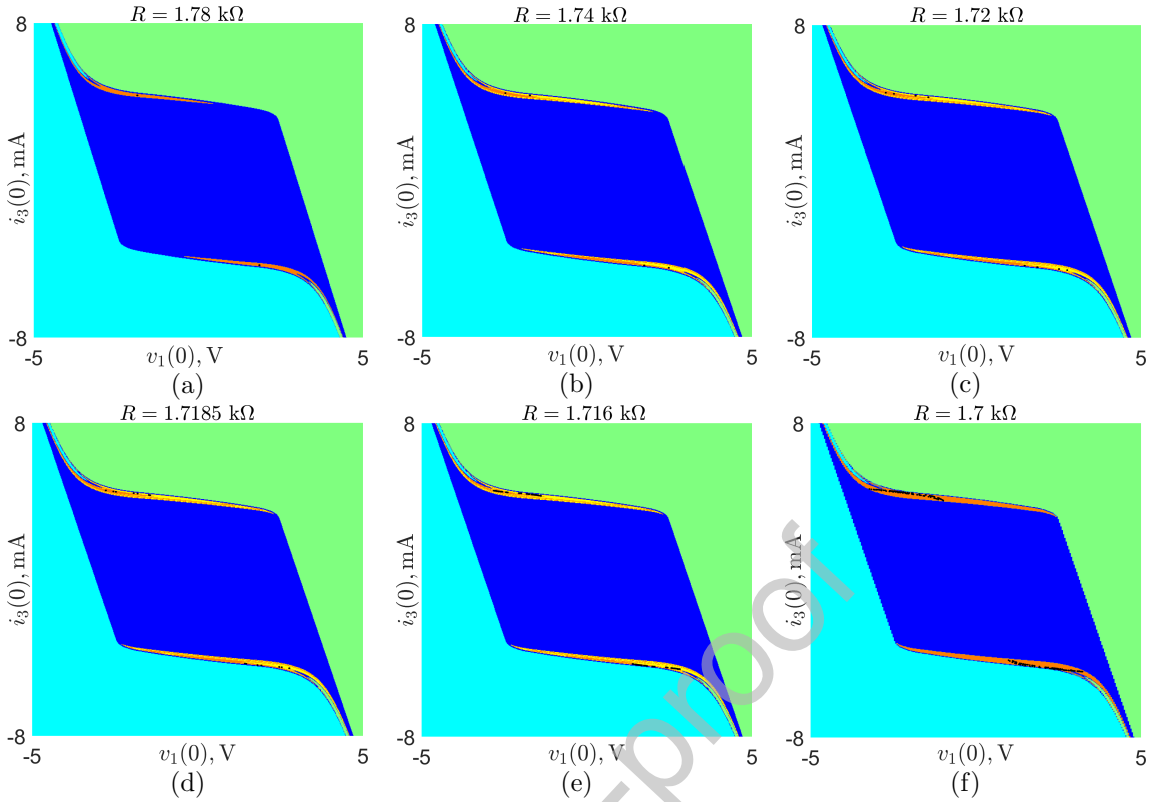

Figure 8: General view of attraction basins in the section $v_2(0) = 0$, where the cyan, green, and blue basins correspond to the point attractors located in the equilibria S_4, S_3, and S_0, respectively. The orange/yellow basins with black cross trajectories correspond to hidden attractors. Coexistence of three point attractors with **(a)** one hidden period-1 limit cycle for $R = 1.78\,\mathrm{k\Omega}$ (b) two symmetric hidden period-1 limit cycles for $R = 1.74\,\mathrm{k\Omega}$ **(c)** two symmetric hidden period-2 limit cycles for $R = 1.72\,\mathrm{k\Omega}$ **(d)** two symmetric hidden period-4 limit cycles for $R = 1.7185\,\mathrm{k\Omega}$ **(e)** two symmetric hidden chaotic attractors for $R = 1.716\,\mathrm{k\Omega}$ **(f)** one hidden chaotic attractor for $R = 1.7\,\mathrm{k\Omega}$.

basins located far away from all equilibria. It is difficult, at least for the time being, to accurately validate the hidden attractors. In this section, we first use PSIM to verify the hidden attractors. Furthermore, DSP-assisted validations are presented as the complement for experiments.

4.1. PSIM simulations

With the schematic diagram of Fig. 1, an analog electronic circuit model is built in PSIM 9.0.3, as shown in Fig. 10. The setup of 'Simulation Control' is $Timestep = 0.2\,\mu\mathrm{s}$, $Totaltime = 0.1\,\mathrm{s}$, and $Printtime = 50\,\mathrm{ms}$, respectively. The 'Voltage Vs+' and 'Voltage Vs-' for the op-amps are $13\,\mathrm{V}$ and $-13\,\mathrm{V}$, respectively.

With the parameters and initial values of Fig. 10, the circuitry simulation results of phase portraits and the time sequences of three variables are shown in Fig. 11. Fix other parameters in Table 1 and set R as $1.78\,\mathrm{k\Omega}$, $1.74\,\mathrm{k\Omega}$, $1.72\,\mathrm{k\Omega}$, $1.7185\,\mathrm{k\Omega}$, $1.716\,\mathrm{k\Omega}$, and $1.7\,\mathrm{k\Omega}$, the circuitry simulation results are shown in Fig. 12(a)-(f), where the magenta and black orbits are excited by initial values $(0\,\mathrm{V}, 1.9\,\mathrm{V}, 0\,\mathrm{A})$ and $(0\,\mathrm{V}, -1.9\,\mathrm{V}, 0\,\mathrm{A})$, respectively. It is seen that the transitions from period-1 limit cycle to chaotic attractor indicate a identical period-doubling bifurcation route to chaos. The circuit simulation results are consistent well with the numerical analyses.

It is noted that numerical simulations of nonlinear ODEs systems suffer from errors due to time discretization, and only the trajectories over a finite-time interval can be simulated [27, 33]. PSIM, as well as any other simulator, also suffer from discretization effect, i.e., finite tolerance [24, 30]. In this

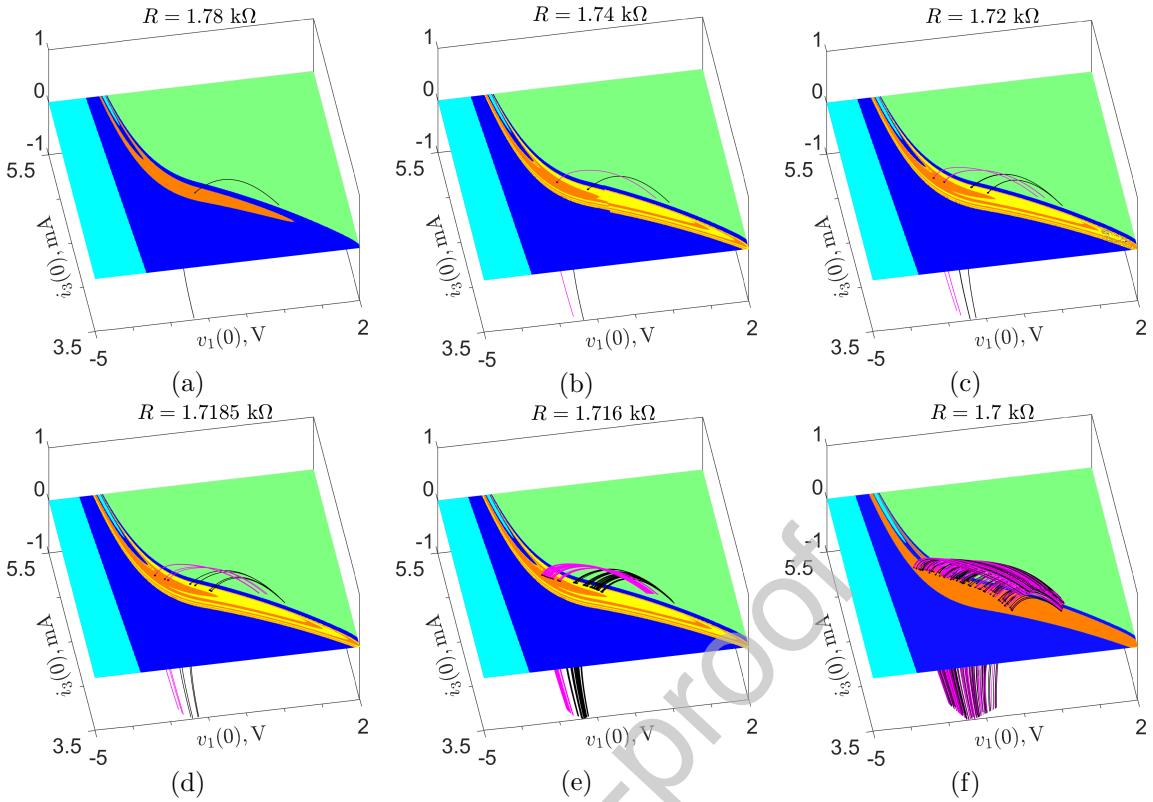

Figure 9: Local view of hidden attractors overplotted on corresponding basins for **(a)** $R = 1.78\,\mathrm{k\Omega}$ **(b)** $R = 1.74\,\mathrm{k\Omega}$ **(c)** $R = 1.72\,\mathrm{k\Omega}$ **(d)** $R = 1.7185\,\mathrm{k\Omega}$ **(e)** $R = 1.716\,\mathrm{k\Omega}$ **(f)** $R = 1.7\,\mathrm{k\Omega}$.

contribution, a large number of simulations performed on PSIM show that discretization has limited influence for finite-time dynamics with $Timestep \leq 0.2\,\mu\mathrm{s}$.

4.2. DSP-assisted experiments

Additionally, the system model of (6) is implemented by using DSP. The system (6) is first discretized by the fourth-order Runge-Kutta algorithm (the specific discretization process can refer to [34]). The isolated emulator YXDSP-XDS100V3 in tandem with core DSP processing chip TMS320F28335 are used for programming and emulation. In combination with the D/A converter DAC8552, two output signal can be measured by the probes of digital oscilloscope. With the X-Y display mode, the experimental result of hidden chaotic attractor is captured, as shown in Fig. 13. Moreover, with different R and initial conditions, the phase portraits of periodic limit cycle, twin hidden attractors, and the typical hidden chaotic attractors are measured and shown in Fig. 14(a)-(j), respectively. The DSP-assisted experimental results are consistent with that obtained via numerical simulations and circuitry simulations, which validate the existence of hidden attractors and coexisting attractors.

5. Conclusion

In this paper, the design and dynamics analysis of a modified Chua's circuit have been presented. First, by using two nonlinear resistors, a 5-segment piecewise-linear Chua's diode was designed. The slopes of the inner three segments satisfy $G_b < G_a < 0$ and have the identical characteristics with the Chua's nonlinearity proposed in [16]. With this Chua's diode, a modified Chua's circuit with five equilibria including three stable node-foci and two unstable saddles was further implemented. Rich dynamical behaviors such as bifurcation and chaos were investigated by bifurcations diagrams and Lyapunov exponents. In addition to these dynamics, the multistability phenomena of coexisting hidden attractors with point attractors were

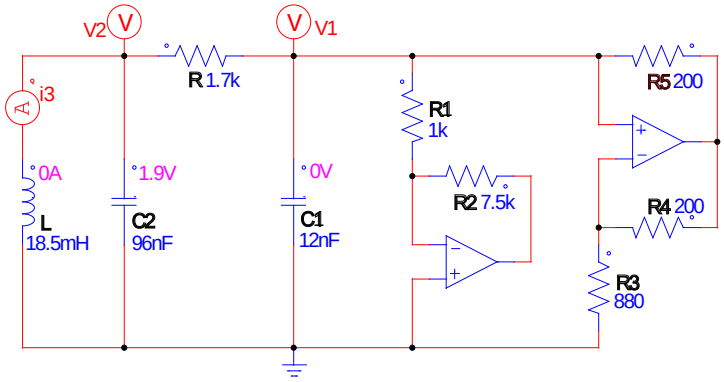

Figure 10: Modified Chua's circuit built in PSIM

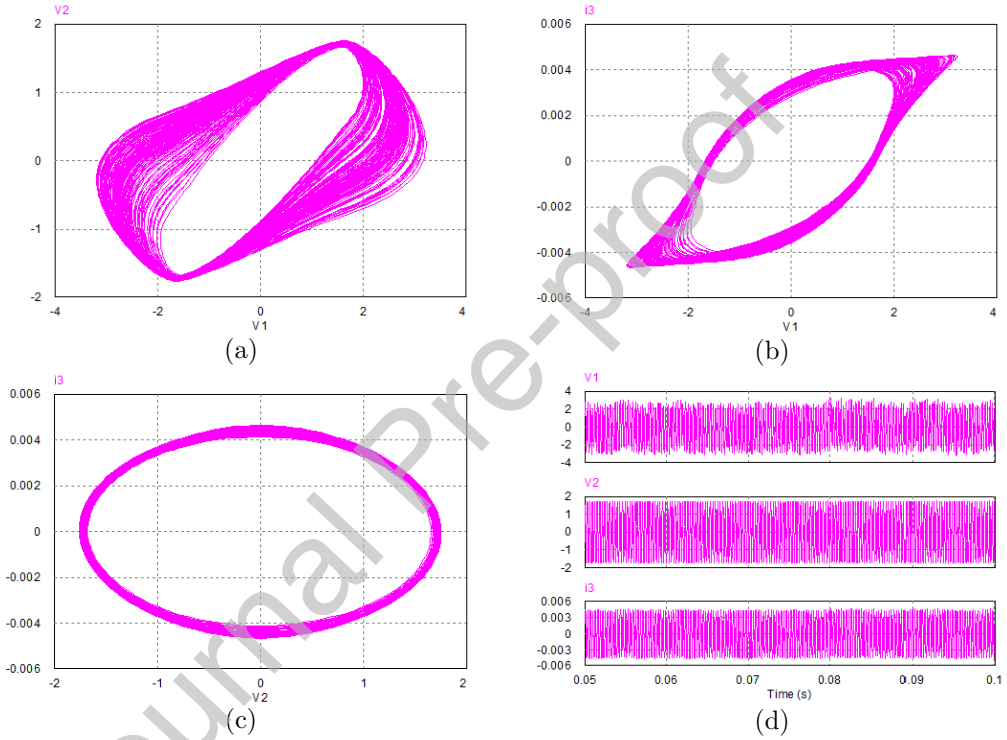

Figure 11: PSIM simulations of hidden chaotic attractor. **(a)** phase portrait in $v_1 - v_2$ plane **(b)** phase portrait in $v_1 - i_3$ plane **(c)** phase portrait in $v_2 - i_3$ plane **(d)** time sequences of $v_1(t)$, $v_2(t)$, and $i_3(t)$.

also noticed in the entire period-doubling bifurcation route. Up to five coexisting attractors including three point attractors and two symmetric hidden attractors can be generated in this Chua's circuit. It was also demonstrated that the hidden attractors have very small basins of attraction not being connected with any fixed point. Besides, the existence of hidden attractors and coexisting attractors have been validated by the PSIM circuit simulations and DSP-assisted experiments.

Some open problems deserve further study. For examples, what is the maximum number of coexisting attractors (including the self-excited and hidden attractors) that can be generated in the Chua's system [25], what is the application prospect for hidden chaotic dynamics in chaos-based secure communications [35], and how to achieve an effective experimental method for validations of hidden attractors, et al.

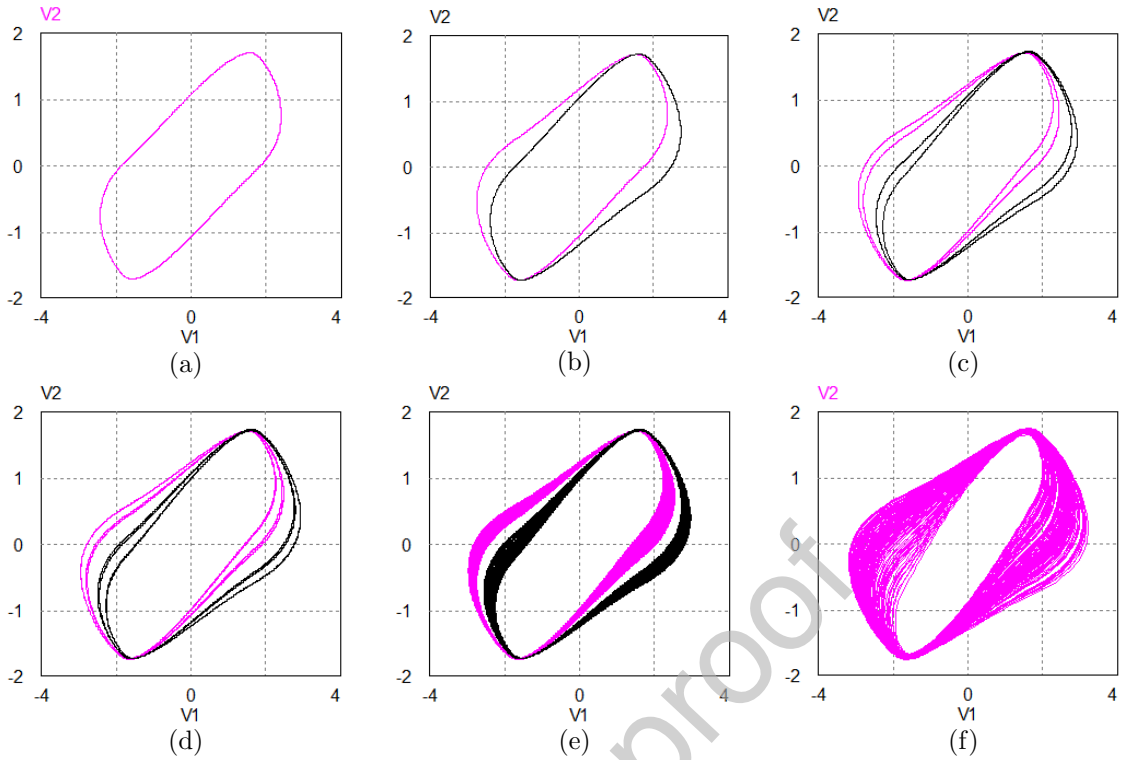

Figure 12: PSIM simulations of hidden attractors for different R, where the parameters in Table 1 are used. The attractors marked with magenta and black are excited from ICs $(0\,\mathrm{V}, 1.9\,\mathrm{V}, 0\,\mathrm{A})$ and $(0\,\mathrm{V}, -1.9\,\mathrm{V}, 0\,\mathrm{A})$, respectively. **(a)** period-1 limit cycle for $R = 1.78\,\mathrm{k\Omega}$ **(b)** twin period-1 limit cycles for $R = 1.74\,\mathrm{k\Omega}$ **(c)** twin period-2 limit cycles for $R = 1.72\,\mathrm{k\Omega}$ **(d)** twin period-4 limit cycles for $R = 1.7185\,\mathrm{k\Omega}$ **(e)** twin chaotic attractors for $R = 1.716\,\mathrm{k\Omega}$ **(f)** chaotic attractor for $R = 1.7\,\mathrm{k\Omega}$.

CRediT authorship contribution statement

Ning Wang: Methodology, Formal analysis, and Writing- Original draft preparation. Guoshan Zhang: Supervision, Investigation, Writing- Reviewing and Editing. Kuznetsov N. V.: Supervision, Investigation, Writing- Reviewing and Editing. Han Bao: Figures production.

Declaration of Competing Interest

The authors declare that they have no known competing financial interests or personal relationships that could have appeared to influence the work reported in this paper.

Acknowledgments

This work was supported by the National Natural Science Foundation of China under Grant No. 61473202, and the Russian Science Foundation 19-41-02002 (hidden attractors). Ning Wang (CSC No. 202006250146) would like to acknowledge the sponsor from China Scholarship Council.

References

[1] G. A. Leonov, N. V. Kuznetsov, Hidden attractors in dynamical systems. From hidden oscillations in Hilbert-Kolmogorov, Aizerman, and Kalman problems to hidden chaotic attractor in Chua circuits, International Journal of Bifurcation and Chaos 23 (1) (2013) 1330002. doi:10.1142/S0218127413300024.

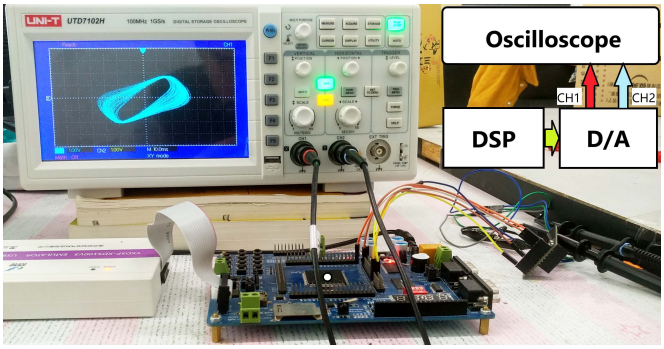

Figure 13: DSP-based implementation and the hidden chaotic attractor.

[2] D. Dudkowski, S. Jafari, T. Kapitaniak, N. V. Kuznetsov, G. A. Leonov, A. Prasad, Hidden attractors in dynamical systems, Physics Reports 637 (2016) 1–50. doi:10.1016/j.physrep.2016.05.002.

[3] T. Kapitaniak, G. A. Leonov, Multistability: Uncovering hidden attractors, European Physical Journal Special Topics 224 (8) (2015) 1405–1408. doi:10.1140/epjst/e2015-02468-9.

[4] X. Wang, G. Chen, A chaotic system with only one stable equilibrium, Communications in Nonlinear Science and Numerical Simulation 17 (3) (2012) 1264–1272. doi:10.1016/j.cnsns.2011.07.017.

[5] J. C. Sprott, X. Wang, G. Chen, Coexistence of point, periodic and strange attractors, International Journal of Bifurcation and Chaos 23 (05) (2013) 1350093. doi:10.1142/S0218127413500934.

[6] Z. Wei, I. Moroz, J. C. Sprott, A. Akgul, W. Zhang, Hidden hyperchaos and electronic circuit application in a 5D self-exciting homopolar disc dynamo, Chaos 27 (3) (2017) 033101. doi:10.1063/1.4977417.

[7] B. Bao, H. Bao, N. Wang, M. Chen, Q. Xu, Hidden extreme multistability in memristive hyperchaotic system, Chaos, Solitons & Fractals 94 (2017) 102–111. doi:10.1016/j.chaos.2016.11.016.

[8] V.-T. Pham, S. Jafari, C. Volos, T. Kapitaniak, Different families of hidden attractors in a new chaotic system with variable equilibrium, International Journal of Bifurcation and Chaos 27 (09) (2017) 1750138. doi:10.1142/S0218127417501383.

[9] M.-F. Danca, M. Fečkan, Hidden chaotic attractors and chaos suppression in an impulsive discrete economical supply and demand dynamical system, Communications in Nonlinear Science and Numerical Simulation 74 (2019) 1–13. doi:10.1016/j.cnsns.2019.03.008.

[10] J. P. Singh, B. K. Roy, N. V.Kuznetsov, Multistability and hidden attractors in the dynamics of permanent magnet synchronous motor, International Journal of Bifurcation and Chaos 29 (4) (2019) 1950056. doi:10.1142/S0218127419500561.

[11] S. Jafari, J. C. Sprott, F. Nazarimehr, Recent new examples of hidden attractors, European Physical Journal Special Topics 224 (8) (2015) 1469–1476. doi:10.1140/epjst/e2015-02472-1.

[12] Y. Yang, G. Qi, J. Hu, P. Faradja, Finding method and analysis of hidden chaotic attractors for plasma chaotic system from physical and mechanistic perspectives, International Journal of Bifurcation and Chaos 30 (5) (2020) 2050072. doi:10.1142/S0218127420500728.

[13] L. Fortuna, M. Frasca, M. G. Xibilia, Chua's Circuit Implementations: Yesterday, Today and Tomorrow, Signapore: World Scientific, 2009. doi:10.1142/7200.

[14] N. V. Kuznetsov, G. A. Leonov, V. I. Vagaitsev, Analytical-numerical method for attractor localization of generalized Chua's system, IFAC Proceedings Volumes 43 (11) (2010) 29–33. doi:10.3182/20100826-3-TR-4016.00009.

[15] G. A. Leonov, N. V. Kuznetsov, Analytical-numerical methods for investigation of hidden oscillations in nonlinear control systems, IFAC Proceedings Volumes 44 (1) (2011) 2494–2505. doi:10.3182/20110828-6-IT-1002.03315.

[16] G. A. Leonov, N. V. Kuznetsov, V. I. Vagaitsev, Localization of hidden Chua's attractors, Physics Letters A 375 (23) (2011) 2230–2233. doi:10.1016/j.physleta.2011.04.037.

[17] G. A. Leonov, N. V. Kuznetsov, V. I. Vagaitsev, Hidden attractor in smooth Chua systems, Physica D 241 (18) (2012) 1482–1486. doi:10.1016/j.physd.2012.05.016.

[18] Q. Li, H. Zeng, X. Yang, On hidden twin attractors and bifurcation in the Chua's circuit, Nonlinear Dynamics 77 (2014) 255–266. doi:10.1007/s11071-014-1290-8.

[19] H. Zhao, Y. Lin, Y. Dai, Hopf bifurcation and hidden attractor of a modified Chua's equation, Nonlinear Dynamics 90 (2017) 2013–2021. doi:10.1007/s11071-017-3777-6.

[20] B. Bao, F. Hu, M. Chen, Q. Xu, Y. Yu, Self-excited and hidden attractors found simultaneously in a modified Chua's circuit, International Journal of Bifurcation and Chaos 25 (5) (2015) 1550075. doi:10.1142/S0218127415500753.

[21] B. Bao, P. Jiang, Q. Xu, M. Chen, Hidden attractors in a practical Chua's circuit based on a modified Chua's diode, Electronics Letters 52 (1) (2016) 23–25. doi:10.1049/el.2015.2493.

[22] B. Bao, Q. Li, N. Wang, Q. Xu, Multistability in Chua's circuit with two stable node-foci, Chaos 26 (4) (2016) 043111. doi:10.1063/1.4946813.

[23] M. Chen, Q. Xu, Y. Lin, B. Bao, Multistability induced by two symmetric stable node-foci in modified canonical Chua's circuit, Nonlinear Dynamics 87 (2017) 789–802. doi:10.1007/s11071-016-3077-6.

[24] M. A. Kiseleva, E. V. Kudryashova, N. V. Kuznetsov, O. A. Kuznetsova, G. A. Leonov, M. V. Yuldashev, R. V. Yuldashev, Hidden and self-excited attractors in Chua circuit: synchronization and SPICE simulation, International Journal of Parallel, Emergent and Distributed Systems 33 (5) (2018) 513–523. doi:10.1080/17445760.2017.1334776.

[25] N. V. Stankevich, N. V. Kuznetsov, G. A. Leonov, L. O. Chua, Scenario of the birth of hidden attractors in the Chua circuit, International Journal of Bifurcation and Chaos 27 (12) (2017) 1730038. doi:10.1142/S0218127417300385.

[26] N. Wang, C. Li, H. Bao, M. Chen, B. Bao, Generating multi-scroll Chua's attractors via simplified piecewise-linear Chua's diode, IEEE Transactions on Circuits and Systems–I: Regular Papers 66 (12) (2019) 4767–4779. doi:10.1109/TCSI.2019.2933365.

[27] M.-F. Danca, P. Bourke, N. V. Kuznetsov, Graphical structure of attraction basins of hidden chaotic attractors: The Rabinovich-Fabrikant system, International Journal of Bifurcation and Chaos 29 (1) (2019) 1930001. doi:10.1142/S0218127419300015.

[28] N. Wang, G. Zhang, H. Bao, Bursting oscillations and coexisting attractors in a simple memristor-capacitor-based chaotic circuit, Nonlinear Dynamics 97 (2019) 1477–1494. doi:10.1007/s11071-019-05067-6.

[29] J. Ma, X. Wu, R. Chu, L. Zhang, Selection of multi-scroll attractors in jerk circuits and their verification using Pspice, Nonlinear Dyn. 76 (4) (2014) 1951–1962. doi:10.1007/s11071-014-1260-1.

[30] N. V. Kuznetsov, G. A. Leonov, M. V. Yuldashev, R. V. Yuldashev, Hidden attractors in dynamical models of phase-locked loop circuits: Limitations of simulation in MATLAB and SPICE, Communications in Nonlinear Science and Numerical Simulation 51 (2017) 39–49. doi:10.1016/j.cnsns.2017.03.010.

[31] Q. Lai, Z. Wan, P. Kuate, F. Hilaire, Coexisting attractors, circuit implementation and synchronization control of a new chaotic system evolved from the simplest memristor chaotic circuit, Communications in Nonlinear Science and Numerical Simulation 89 (2020) 105341. doi:10.1016/j.cnsns.2020.105341.

[32] H. Bao, N. Wang, B. Bao, M. Chen, P. Jin, G. Wang, Initial condition-dependent dynamics and transient period in memristor-based hypogenetic jerk system with four line equilibria, Communications in Nonlinear Science and Numerical Simulation 57 (2018) 264–275. doi:10.1016/j.cnsns.2017.10.001.

[33] N. V. Kuznetsov, G. A. Leonov, T. N. Mokaev, A. Prasad, M. D. Shrimali, Finite-time Lyapunov dimension and hidden attractor of the Rabinovich system, Nonlinear Dynamics 92 (2018) 267–285. doi:10.1007/s11071-018-4054-z.

[34] N. Wang, G. Zhang, H. Bao, Infinitely many coexisting conservative flows in a 4D conservative system inspired by LC circuit, Nonlinear Dynamics 99 (2020) 3197–3216. doi:10.1007/s11071-020-05465-1.

[35] C. Li, Y. Zhang, E. Y. Xie, When an attacker meets a cipher-image in 2018: A year in review, Journal of Information Security and Applications 48 (2019) 102361. doi:10.1016/j.jisa.2019.102361.

Figure 14: Experimental phase portraits of hidden attractors for different R, where the resistances and initial conditions are given in corresponding sub-figures **(a)** period-1 limit cycle **(b)** hidden chaotic attractor **(c)** left (twin) period-1 limit cycle **(d)** right (twin) period-1 limit cycle **(e)** left (twin) period-2 limit cycles **(f)** right (twin) period-2 limit cycle **(g)** left (twin) period-4 limit cycle **(g)** right (twin) period-4 limit cycle **(i)** left (twin) chaotic attractors **(j)** right (twin) chaotic attractors.

Declaration of interests

☒ The authors declare that they have no known competing financial interests or personal relationships that could have appeared to influence the work reported in this paper.

☐The authors declare the following financial interests/personal relationships which may be considered as potential competing interests:

CRediT authorship contribution statement Ning Wang: Methodology, Formal analysis, and Writing- Original draft preparation. Guoshan Zhang: Supervision, Investigation, Writing- Reviewing and Editing. Kuznetsov N. V.: Supervision, Investigation, Writing- Reviewing and Editing. Han Bao: Figures production.